高分辨率高效率三维正电子发射断层扫描成像探测器研发

李 成[1] 邝忠华[1] 都军伟[2] 白晓薇[2] Simon R. Cherry[2]
梁 栋[1] 刘 新[1] 郑海荣[1] 杨永峰[1]

[1](中国科学院深圳先进技术研究院 深圳 518055)
[2](美国加州大学戴维斯分校生物医学工程系 加利福尼亚 95616)

摘 要 小动物正电子发射断层扫描成像(Positron Emission Tomography，PET)是临床前生物医学研究的重要工具，但小动物 PET 要同时达到高空间分辨率和高效率必须使用三维深度测量探测器。本工作使用位置灵敏雪崩光二极管(Position-Sensitive Avalanche Photodiode，PSAPD)和位置灵敏硅光电倍增管(Position-Sensitive Silicon Photomultipliers，PS-SiPM)双端读出，测量了晶体大小为 0.7～0.44 mm 的高分辨率硅酸镥晶体阵列，其中对一种最新研发成功的 PS-SiPM 进行了首次测试。首先对 PS-SiPM 和 PSAPD 的信噪比进行了测量，然后对使用 PS-SiPM 和 PSAPD 的双端读出探测器模块的晶格分辨图、能量分辨率和相互作用深度分辨率分别进行了测量。实验发现，PSAPD 的信噪比远远优于 PS-SiPM，使用 PSAPD 的探测器可以分辨 0.44 mm 的晶格阵列和最好达到 1.4 mm 的深度分辨率，而使用 PS-SiPM 的探测器模块可以分辨 0.7 mm 的硅酸镥晶体阵列和达到 2.9 mm 的深度分辨率。从得到的晶格分辨图、能量分辨率和相互作用深度分辨率上来看，使用 PSAPD 的探测器模块要优于使用 PS-SiPM 的探测器。这需要提高 PS-SiPM 的信噪比来进一步提高探测器分辨更小截面晶格的能力，提高 PS-SiPM 微单元的数量来降低饱和效应从而提高探测器的相互作用深度分辨率。从实验结果可以看出，基于 PSAPD 的三维相互作用深度测量 PET 探测器具有更好的性能，今后计划使用新的 PS-SiPMs 和 SiPM 阵列进行该类型探测器的研发。

关键词 小动物正电子发射断层扫描成像；探测器；雪崩光二极管；硅光电倍增管
中图分类号 R 318.6 **文献标志码** A

Received: 2015-04-04 **Revised:** 2016-06-01
Foundation: National Natural Science Foundation (81527804, 11575285); Natural Science Foundation of Guangdong Province (2014A030312006)
Author: LI Cheng, Ph.D, Postdoctoral Fellow, his research interests include PET detector, electronics and system. KUANG Zhonghua, Master degree student, his research interests include PET detector measurement and data analysis. DU Junwei, Ph.D, Associate Specialist, his research interests include PET detector and electronics. BAI Xiaowei, Staff Research Associate, her research interests include PET electronics and system integration. Simon R. Cherry, Ph.D, Distinguished Professor, his research interests include molecular imaging instrumentation and application. LIANG Dong, Ph.D, Professor, his research interests include CT and MRI imaging. LIU Xin, Ph.D, Professor, his research interests include MRI instrumentation and application. ZHEGN Hairong, Ph.D, Professor, his research interests include ultrasound instrumentation and application. YANG Yongfeng (corresponding author), Ph.D, his research interests include PET and PET/MRI instrumentation, E-mail: yf.yang@siat.ac.cn.

High Spatial Resolution and High Sensitivity Three Dimensional PET Detector Development with Position-sensitive Avalanche Photodiode and Silicon Photomultiplier Readout

LI Cheng[1] KUANG Zhonghua[1] DU Junwei[2] BAI Xiaowei[2] Simon R. Cherry[2]

LIANG Dong[1] LIU Xin[1] ZHENG Hairong[1] YANG Yongfeng[1]

[1](*Shenzhen Institutes of Advanced Technology*, *Chinese Academy of Sciences*, *Shenzhen* 518055, *China*)

[2](*Department of Biomedical Engineering*, *University of California-Davis*, *CA* 95616, *USA*)

Abstract Small animal positron emission tomography (PET) is a well-established imaging modality in preclinical biomedical research. But depth encoding detectors are required to simultaneously achieve high spatial resolution and high sensitivity for a small animal PET scanner. In this work, we evaluated several dual-ended readout detector modules using lutetium oxyorthosilicate (LSO) arrays with crystal sizes ranging from 0.70 mm to 0.44 mm, read out by either position-sensitive avalanche photodiodes (PSAPDs) or position-sensitive silicon photomultipliers (PS-SiPMs). A new type of PS-SiPM was developed recently and was evaluated for the first time in this work. First, the signal-to-noise ratio (SNR) of both PSAPDs and PS-SiPMs was measured, and then the flood histograms, energy resolution and depth of interaction (DOI) resolution of dual-ended readout detector modules by using both PSAPDs and PS-SiPMs were measured. The PSAPD has much better SNR as compared with PS-SiPM. For the detectors using PSAPDs, crystals as small as 0.44 mm can be resolved and a DOI resolution as good as 1.4 mm was obtained. For the detectors using PS-SiPMs, 0.7 mm crystals can be resolved and a DOI resolution of 2.9 mm was obtained. Based on the results of the flood histograms, energy resolution and DOI resolution the detector modules using PSAPD are better than those using PS-SiPMs. The SNR of the PS-SiPM would need to be improved to resolve even smaller crystals and the number of SiPM cells also need to be increased to reduce the saturation effect to improve the DOI resolution. The performance of the three dimensional depth encoding PET detectors using PSAPDs is much better because the SNR of PSAPD is much higher than PS-SiPM. In the future, high resolution depth encoding PET detectors will be developed by using both new PS-SiPMs and SiPM arrays.

Keywords small animal PET; detector; avalanche photodiode; silicon photomultiplier

1 Introduction

Positron emission tomography (PET) is a well-established imaging modality in model biomedical research and clinical diagnosis. Small animal PET is one of the imaging modalities that offer considerable potential in animal models of human disease research and new drug and therapy development. The main barriers to using clinical PET scanners in studies of laboratory animals have traditionally been poor spatial resolution, poor signal-to-noise, cost and accessibility. Academic groups and industry have been addressing these issues for about two decades[1-5], with the result that compact, lower-cost laboratory animal PET scanners, with much improved spatial resolution and sensitivity have

become available. Presently, it is estimated that there are over 500 small animal PET scanners installed worldwide. PET is clearly an established modality for preclinical studies.

Despite substantial advances in small-animal PET technology, image quality, as defined by spatial resolution and signal-to-noise ratio (SNR), remains well below what can be achieved theoretically. The reconstructed resolution of current commercial small-animal PET systems typically falls in the 1-2 mm range. Volumetrically this translates to between 1 and 8 μL. In most current small animal PET scanners, a compromise between sensitivity and spatial resolution has to make due to the depth of interaction (DOI) effect. Typically, much shorter crystals (about 10 mm thick compared to 20-30 mm for a clinical scanner) are used for a small animal PET scanner[6] and the ring diameter is kept larger than needed, but still the spatial resolution degrades rapidly as you move away from the center of the field of view, even if advanced reconstruction algorithms that model the crystal penetration are used[7]. DOI effects are the single biggest limitation in improving the resolution/sensitivity trade-off in small-animal PET. For this reason, much attention in recent years has focused on detector designs with depth-encoding ability. DOI encoding techniques include multi-layer detectors consisting of crystal layers with different scintillation light decay times[8-11], with different reflector arrangements[12,13], and using a position shift of half a crystal for different layers[14], dual-ended readout of scintillator arrays[15-18], measuring charge collection time differences at the cathode and the anode for semiconductor detectors[19,20], and measuring light distribution with a multi-channel photomultiplier tube (PMT) or silicon photomultiplier array for a continuous crystal scintillator detector[21,22]. Dedicated small animal PET scanners[23] have now been developed that utilize some form of depth-encoding detectors. High resolution depth-encoding detectors have the potential to allow a PET scanner to be built with a smaller ring diameter and/or using longer crystals while maintaining high spatial resolution. Smaller ring diameter means higher sensitivity, lower cost and a smaller photon noncollinearity effect. Longer crystals mean higher sensitivity. Thus solving the DOI problem is the key to the development of higher performance and lower cost small-animal PET scanners.

The length of mice is about one tenth of a human. If one wants to obtain the same relative spatial resolution for mouse imaging as human imaging performed on a 5 mm resolution clinical whole body PET scanner, the required spatial resolution of ~0.5 mm is much higher than that can be achieved with the currently dedicated small animal PET scanner (1-2 mm). Meanwhile high sensitivity is also required to obtain a good SNR of the image to reliably detect lower levels of radiotracer uptake and measure the temporal dynamics of physiological process, and to reduce the injected dose (mass) to animals. Achieving a spatial resolution ~0.5 mm for small animal PET is not only required, but also possible. With ^{18}F, positron range and non-colinearity (10 cm diameter ring) contribute on the order of 0.5 mm blurring to the reconstructed images[24,25], suggesting that reconstructed resolutions approaching to 0.5 mm is possible. This has been approved by a few high resolution prototype small animal PET scanners which used fewer detectors or thinner crystal length, thus only achieved a lower sensitivity[26,27]. Development of depth encoding

PET detectors that can provide high efficiency and high spatial resolution simultaneously is the key factor to improve the performance of small animal PET scanner. In this work, we evaluated several dual-ended readout depth encoding detector modules using lutetium oxyorthosilicate (LSO) arrays with very small crystal sizes ranging from 0.44-0.70 mm, using both position-sensitive avalanche photodiodes (PSAPDs) and a newly developed position-sensitive silicon photomultiplier (PS-SiPM) for readout.

2 Material and methods

2.1 Lutetium oxyorthosilicate array

The detail properties of four LSO arrays used in this work are shown in Table 1. The crystal sizes of LSO arrays are from 0.44 to 0.70 mm. The crystal surfaces of the one LSO array using enhanced specular reflector (ESR) are unpolished (leave as saw cut). The ESR reflector is a 65 μm thin multi-layer polymer film reflector that is 98.5% reflective over the entire visible spectrum, regardless of the angles of the incidence (3M, St. Paul, MN). The ESR is a specular reflector and popularly used in PET detectors. Only one ESR array consisting of unpolished crystal surfaces, 0.7 mm crystal size and 20 mm length was measured in this work since previous results showed that polished crystal surfaces with this reflector could not provide adequate DOI resolution and the edge crystals in one direction cannot be resolved for LSO arrays with this reflector when the crystals size is less than 0.7 mm[28]. For LSO arrays using Toray lumirror E60 film (Toray), three arrays with difference crystal surface, crystal size and length were measured. Toray is a 50 μm thin white microvoided film with excellent opacity (Toray Industries Inc., Japan). A recent study showed that the Toray reflector cannot be described as a specular reflector, a diffuse reflector, nor a linear combination of the two, but instead demonstrates more complex reflection properties[29]. Toray reflector has lower reflectivity as compared to ESR. In addition to the LSO array with unpolished crystal surface, 0.7 mm crystal size and 20 mm length, one LSO array of 0.44 mm crystal size with polished crystal surface and one LSO array of 0.5 mm crystal size with 10 mm length were made to improve light collection so as to unambiguously resolve the small crystal elements. Detector arrays using either reflector have high packing fractions due to their low thickness.

2.2 Position-sensitive avalanche photodiode

The PSAPDs used in this work have a dimension of 10 mm×10 mm and an active area of 8 mm×8 mm. The photography of a PSAPD is shown in Fig. 1. The PSAPDs were developed by Radiation

Table 1 Detailed information of the four LSO arrays measured in this work

(ESR is a specular reflector and Toray is a diffuse paper reflector)

Array #	Crystal element	Crystal size (mm)	Reflector	Crystal surface	Crystal length (mm)
1	10×10	0.70	Toray	unpolished	20
2	10×10	0.70	ESR	unpolished	20
3	14×14	0.44	Toray	polished	20
4	13×13	0.50	Toray	unpolished	10

Monitoring Devices Inc., USA[30]. The back face of the APD consists of a resistive layer with four small corner contacts (anodes) that can provide position information based on comparison of the signal measured at each anode corner. Thus the device produces four position-related signals that vary in a continuous manner for events across the surface of the APD. PSAPDs have been used to develop PET detectors for more than 10 years and their SNR has been continuously improving.

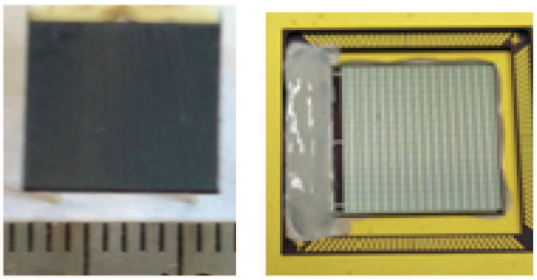

Fig. 1　Photographys of（left）position-sensitive avalanche photodiode and（right）position-sensitive silicon photomultiplier

2.3　Position-sensitive silicon photomultiplier

A new type of PS-SiPM as shown in Fig. 1 was also developed by Radiation Monitoring Devices Inc. recently and is evaluated for the first time in this work. The whole device has an active area of 10.6 mm× 10.1 mm and is separated into 19×18 pixels of 0.5 mm×0.5 mm with 60 μm gaps in between. Each pixel consists of 121 SiPM cells of 30 μm×30 μm. The fill factor within each pixel is 44% and the fill factor of the whole device is 35%. All SiPM cells within the same pixel are connected together and the different pixels are connected with a resistive network. This is different from Radiation Monitoring Devices Inc's previous PS-SiPM devices, in which each microcell was connected to the resistive network[31]. The resistive network circuit used in this device is the same as the previous devices. The whole device is read out by four position-encoding energy signals, the same as a PSAPD. One advantage of the PS-SiPM is that its bias voltage is only ~ 30 V as compared to ~1800 V for PSAPD, also the gain is much higher.

2.4　The measurements

Firstly, the SNR of both PSAPD and PS-SiPM was measured with the same method as described in reference[32] at two different temperatures. The experimental setup used for flood histograms, energy resolution and DOI resolution measurements is shown in Fig. 2. The LSO arrays were read out by placing a photodetector at each end. The dual-ended readout detector modules were placed in a black box which was cooled by sending cool air with an Air-Jet Crystal Cooler (FTS System, Inc., Stone Ridge, NY) to ensure a stable operating temperature. The detector modules were measured in both singles

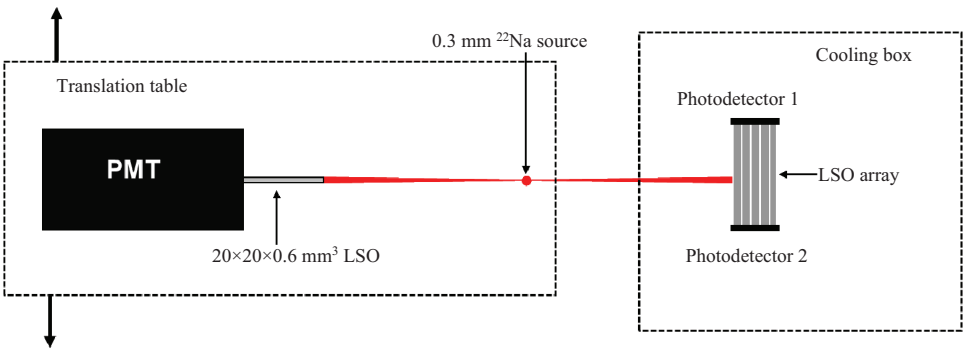

Fig. 2　Experimental setup for flood histogram, energy resolution and depth of interaction resolution measurements

and coincidence modes. In singles modes the entire detector was uniformly radiated by a 0.3 mm ^{22}Na source from one side. In coincidence mode, a specific depth of the detectors was selectively radiated by electric collimation using a 0.6 mm slab detector and the point source placed on a translational stage. The distances from the point source to both detectors are 5 cm. The radiation beam width on LSO arrays for the DOI resolution measurement is about 0.6 mm. For LSO array 1-3, five depths of 2, 6, 10, 14 and 18 mm from one photodetector were measured. For LSO array 4, the measurement was only performed by using PSAPD at 4 depths of 2, 4, 6 and 8 mm.

The schematics of the electronics system for the coincidence measurement is shown in Fig. 3. Standard nuclear instrument module electronics were used. The timing signals from the readout boards of both photodetectors were amplified by a timing filter amplifier firstly, then summed by using a linear fan in/out and finally was sent to a constant fraction discriminator. The constant fraction discriminator produced a logic signal that can be used to coincide with the slab detector that was read out by a PMT. The timing signal of the PMT detector was also amplified by a timing filter amplifier firstly, then sent to a constant fraction discriminator, and delayed before being sent to the coincidence unit. The four energy signals from the readout board of each photodetector were amplified by a spectroscopy amplifier. Then the 8 energy signals from the two photodetectors are passed to an eight channel data acquisition board, digitized and stored as list mode data[33]. For singles measurement, the PMT detector is disabled and the coincidence unit was bypassed.

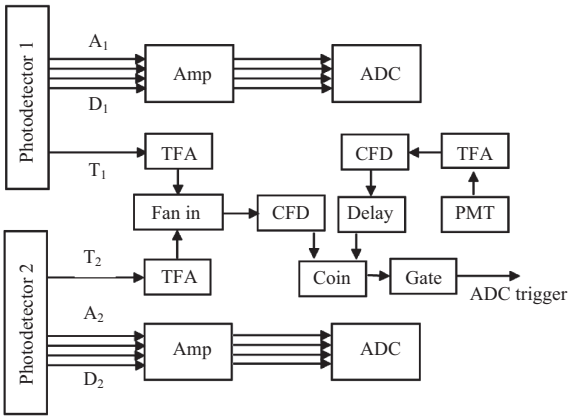

A_1-D_1: the four energy signals of photodetector 1

T_1: the timing signal of photodetector 1

A_2-D_2: the four energy signals of photodetector 2

T_2: the timing signal of photodetector 2

Amp: spectroscopy amplifier Fan in: linear fan in/out

TFA: timing filter amplifier CFD: constant fraction discriminator

COIN: logic coincidence Gate: gate generator

ADC: analogue to digital converter

Fig. 3 Electronics schematic for coincidence measurement

2.5 Data analysis

The energy, flood histogram and DOI calculation method of both PSAPD and PS-SiPM are the same. E_1 and E_2 are the total energy measured by the two photodetectors respectively, and are calculated from the following equations:

$$E_1 = A_1 + B_1 + C_1 + D_1 \quad E_2 = A_2 + B_2 + C_2 + D_2 \quad (1)$$

where A_1, B_1, C_1, and D_1 are the four position-encoding energy signals from photodetector 1 and A_2, B_2, C_2, and D_2 are the four position-encoding energy signals of photodetector 2. For dual-ended readout, the total detected energy (E) was taken to be the sum of the energy measured by the two photodetectors:

$$E = E_1 + E_2 \quad (2)$$

To analyze the data for each dual-ended readout detector either with PSAPD or PS-SiPM, first, a

preliminary flood histogram was obtained from the list mode data measured in singles mode by using a detector-based lower energy threshold corresponding to 150 keV. The x and y coordinates of the flood histograms of the dual-ended readout detectors were calculated using the position-encoding energy signals of the two photodetectors and the following equations:

$$\begin{aligned} x_1&=(B_1+C_1)/E_1 \quad & y_1&=(C_1+D_1)/E_1 \\ x_2&=(B_2+C_2)/E_2 \quad & y_2&=(C_2+D_2)/E_2 \\ x&=(x_1+x_2)/2 \quad & y&=(y_1+y_2)/2 \end{aligned} \tag{3}$$

Second, from the preliminary flood histogram, a crystal look-up table was generated. Then crystal energy spectra for individual crystals in an array were obtained from the singles measurement data using the crystal look-up table. The photopeak amplitudes of individual crystals were obtained by Gaussian fitting of the photopeak of the energy spectra. Finally, a new flood histogram consisting only of events with energy above 350 keV was obtained from the singles data for each array by using a crystal-based lower energy threshold of 350 keV. The spectra of the total energy of all individual crystals in an array were also obtained for the coincidence measurement data. The energy resolution was obtained by Gaussian fitting and the average value will be reported as the energy resolution of each detector module.

The DOI information obtained from the dual-ended readout detector was calculated by using the following formula:

$$DOI\ ratio=\frac{E_2}{E_1+E_2} \tag{4}$$

The histograms of DOI ratios at each of the five measurement depths were obtained for each individual crystal and all crystals in the array from the coincidence measurement data by using the crystal look-up table and a crystal-based lower energy threshold of 350 keV. Then full width at half maximum DOI resolution was calculated by Gaussian fitting of the DOI histograms. The full width at half maximum DOI resolution was then converted to mm by using a linear fit of the peak value of the DOI histograms of all crystals measured at 2 and 18 mm (8 mm for LSO array 4) and the known depth of irradiation.

3 Results

3.1 Signal-to-noise ratio

The signal, noise and SNR of PSAPD and PS-SiPM measured at two temperatures are shown in Fig. 4. For both photodetectors, signal and noise increase as the bias voltage increase. The SNR is relative flat with the changing of bias voltage so a wide range of bias voltage can be used for both photodetectors. The SNR increases as the temperature decreases for both detectors. The SNR of PSAPD is much higher than that of PS-SiPM.

3.2 Detector performance

The flood histograms of all detector modules measured in singles mode are shown in Fig. 5. For all the flood histogram, energy resolution and DOI resolution results measured with PSAPDs and PS-SiPMs, the temperatures are 0℃ and －10℃ respectively. The DOI histograms of all crystals in an array measured in both singles mode and coincidence mode are shown in Fig. 6. The energy resolution and DOI resolution results are summarized in Table 2 and 3. The DOI resolution using “detector calibration” is from DOI histograms of all crystals as shown in Fig. 6. The DOI resolution using “crystal calibration” is obtained from the DOI histograms

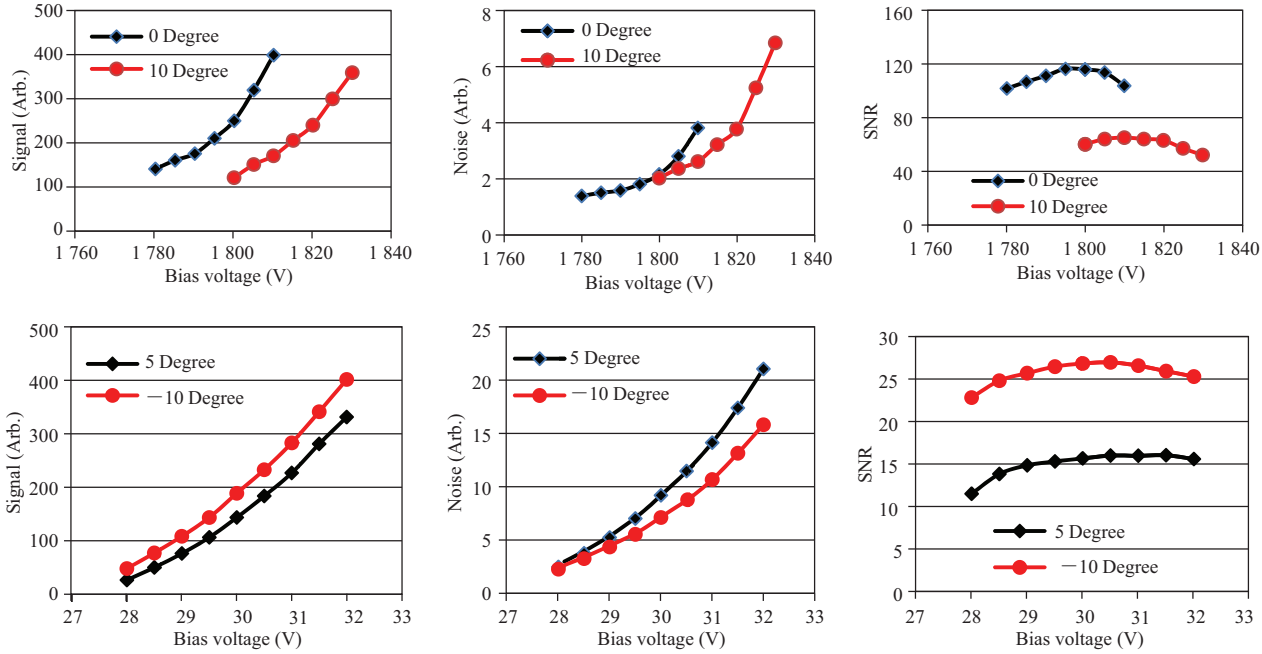

Fig. 4 Signal, noise and signal-to-noise ratio of (top) PSAPD and (bottom) PS-SiPM

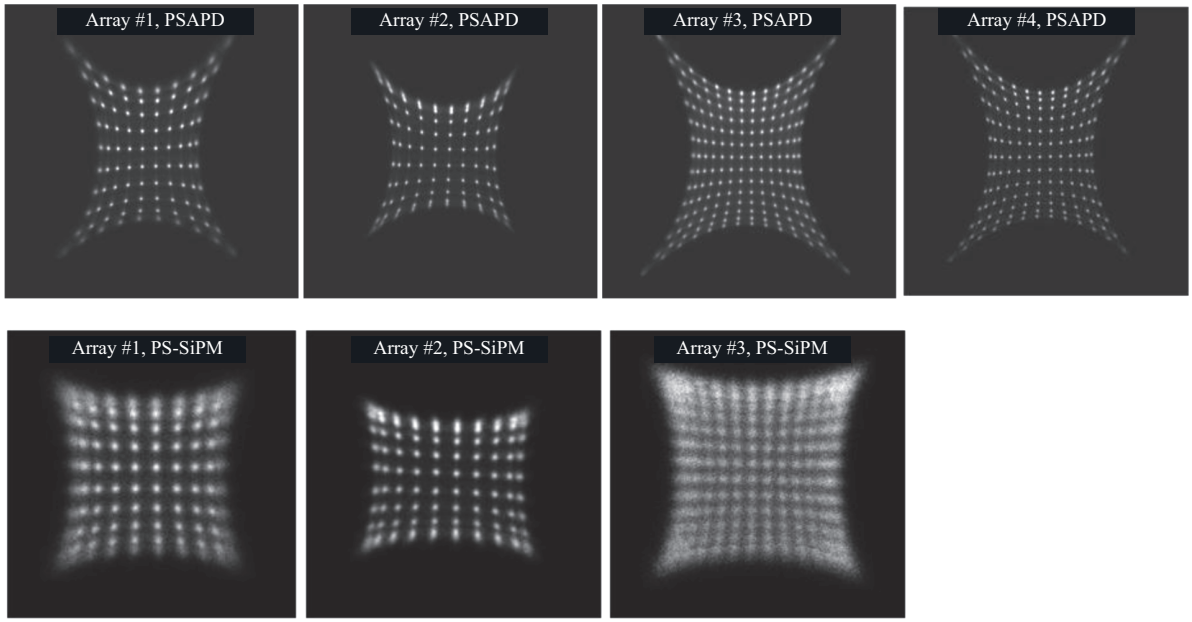

Fig. 5 Flood histograms of all LSO arrays measured in singles mode by dual-ended readout with position-sensitive avalanche photodiodes and position-sensitive silicon photomultipliers

of each individual crystal and Table 3 shows the average of all crystals. The DOI resolution with the crystal calibration is better than that of the detector calibration since there are some DOI ratio variations among crystals, especially among edge and central crystals. The radiation beam width of ~ 0.6 mm was not subtracted from all the DOI resolution results.

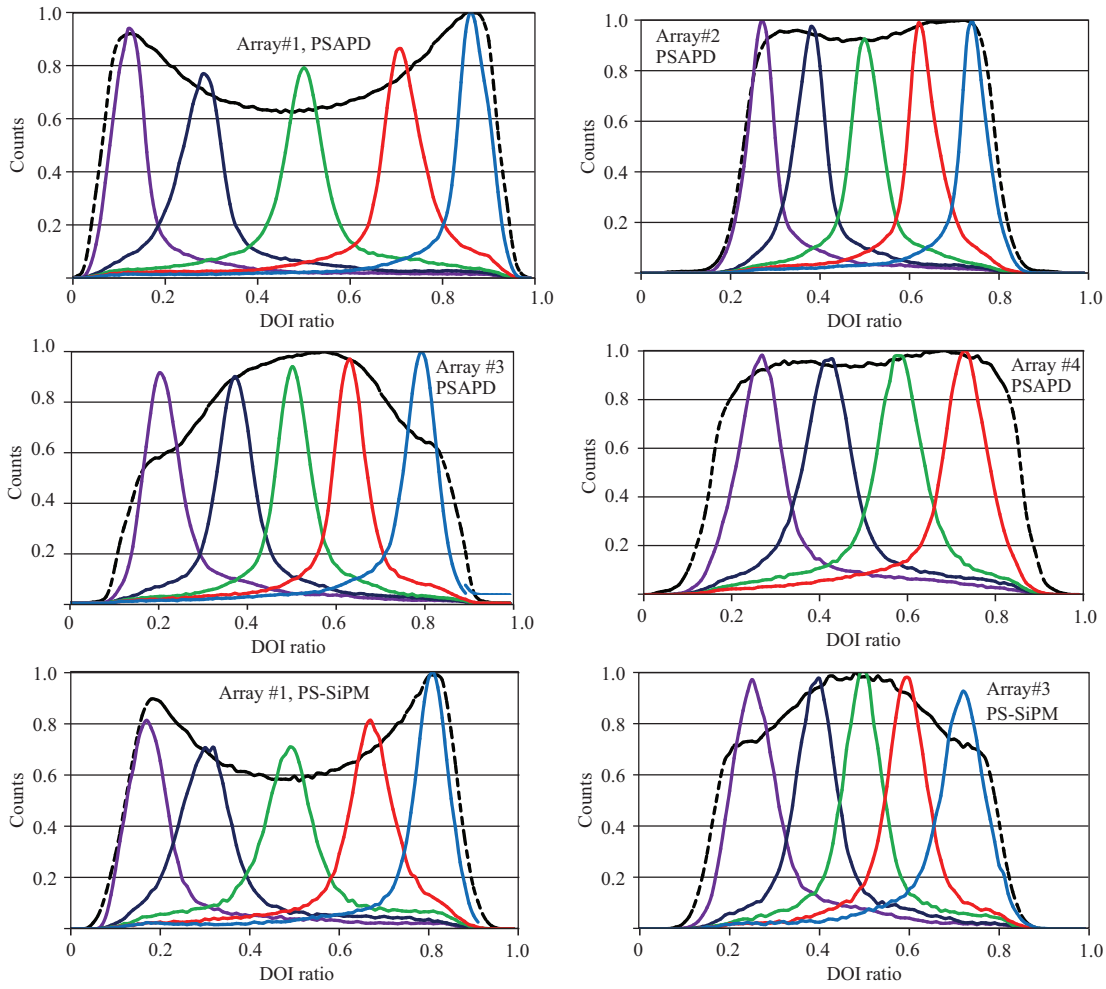

Fig. 6 DOI histograms of the entire array（dish line）and several specific depths of all crystals in an array (Array 1-3 were measured at 5 depths of 2, 6, 10, 14 and 18 mm from one photodetector. Array 4 was measured at 4 depths of 2, 4, 6 and 8 mm)

Table 2　Energy resolution (%) measurement results

Array #	PSAPD(%)	PS-SiPM(%)
1	21.8±3.5	31.8±10.0
2	20.1±4.2	22.9±7.5
3	27.5±5.8	42.4±13.5
4	21.2±5.2	N/A

(1) Position-sensitive silicon photomultiplier vs. position-sensitive avalanche photodiode: PS-SiPM is the first of its type in the world and was made with a novel resistive network readout technology. Unfortunately, it has much lower SNR than PSAPD. The SNR of PS-SiPM at －10℃ is about four times worse than that of PSAPD at 0℃. The flood histograms measured with PS-SiPMs are inferior compared to those measured with PSAPDs. The energy resolution measured with PS-SiPMs is also much worse than that of PSAPDs. There are only 121 cells in each 0.5 mm×0.5 mm pixel for PS-SiPMs. The dynamic range for DOI ratio measured with PS-SiPMs (the results for array 1 and 3 are shown in Fig. 6) is therefore smaller due to the saturation effect. Combining lower SNR and saturation effect, the DOI resolution measured with PS-SiPMs is much worse than that measured with PSAPDs. Although

Table 3 DOI resolution (mm) measurement results

(The DOI resolution using "detector calibration" is from DOI histograms of all crystals. The DOI resolution using "crystal calibration" is obtained from the DOI histograms of each individual crystal and the results are the average of all crystals)

Array #	PSAPD (Detector calibration)	PSAPD (Crystal calibration)	PS-SiPM (Detector calibration)	PS-SiPM (Crystal calibration)
1	2.3	1.6±0.1	3.4	2.9±0.3
2	2.9	1.9±0.2	4.0	3.5±0.4
3	2.8	2.1±0.2	4.2	4.0±0.4
4	1.8	1.4±0.1	N/A	N/A

its performance is not as good as PSAPD, PS-SiPM is still able to resolve 0.7 mm crystals and provides a DOI resolution as high as 2.9 mm, which is good enough for many applications. However, for smaller crystals and better DOI resolution, PSAPDs provide superior performance.

(2) Enhanced specular reflector vs. Toray reflector: ESR is specular reflector with higher reflectivity and Toray reflector is a diffuse reflector with lower reflectivity. Comparing array 1 (using Toray) and 2 (using ESR), array 2 has a smaller dynamic range for the DOI ratio and worse DOI resolution. The flood histogram at center of array 2 appears better than array 1 when PS-SiPMs are used due to the better light collection. From the flood histograms of array 2, two edge rows of the crystals at both top and bottom cannot be resolved no matter which photodetector is used. The flood histogram of array 1 is much better when PSAPDs are used. The energy resolution of LSO array using ESR reflector is better than that of array using Toray reflector. In summary, LSO arrays with Toray reflector provided a better flood histogram and DOI resolution, but worse energy resolution. Energy resolution is less important for small animal PET scanners where the probability of object scattering events is lower.

(3) Polished vs. unpolished crystal surface for Toray arrays: It was shown in the previous work that for LSO array using Toray reflector, unpolished crystal surface, 20 mm long and with 0.5 mm crystal size, the edge crystals cannot be resolved since the light loss is too much[34]. LSO array 3 with Toray reflector and 0.44 mm crystal size was made with polished crystal surface to improve the light collection. The results showed that polishing crystal surface of LSO arrays improves the flood histogram, but reduces the dynamic range of the DOI ratio, thus degrading the DOI resolution. Although the light output of array 3 is ~30% lower than all other arrays (data was not shown), all crystals of array 3 can still be clearly resolved and a DOI resolution of 2.1 mm is obtained with PSAPDs. This detector can be used to build a small animal PET scanner to simultaneously achieve high spatial resolution and high sensitivity.

(4) 10 mm vs. 20 mm long crystals: As compared to 20 mm LSO array, the distance of light photons traveled before reaching the photodetectors is only half for the 10 mm LSO array. All crystals of LSO array 4 using Toray reflector, unpolished crystal surface and 10 mm crystal length can be clearly resolved. Since unpolished crystal surface was used, the DOI ratio change per mm of the array is much larger; it provided the best DOI resolution of 1.4 mm.

But its efficiency is much lower than 20 mm long arrays.

4 Discussion and conclusion

High resolution and high sensitivity dual-ended readout depth-encoding detectors with crystal sizes ranging from 0.7 mm to 0.44 mm, and using both the newly developed PS-SiPMs and PSAPDs, were evaluated. Both photodetectors are compact and can provide very high resolution and continuous spatial information. They are good candidates to develop high resolution dual-ended readout depth-encoding PET detectors. The new PS-SiPM has much lower SNR as compared to PSAPD, 0.7 mm crystals can be resolved and a DOI resolution of 2.9 mm was obtained. The SNR of PS-SiPM needs to be improved to resolve even smaller crystals and improve detector energy resolution, and the number of SiPM cells also needs to be increased to reduce the saturation effect so as to improve the DOI resolution. For detectors using PSAPDs, crystals as small as 0.44 mm can be resolved and a DOI resolution as good as 1.4 mm was obtained. With present technology, PSAPD-based detectors remain the choice for achieving the highest spatial and DOI resolution, but PS-SiPM has advantages such as low bias voltage and high gain, it is will be a promising photodetector for PET application when the SNR is further improved. In the future, we plan to develop high resolution depth encoding PET detectors based on both new PS-SiPMs and SiPM arrays.

For dual-ended readout depth encoding PET detectors, the crystal surface and reflector need to be optimized to find the best balance between flood histogram, energy resolution and DOI resolution. We had shown in our previous work that polished LSO array with ESR reflector cannot provide adequate DOI resolution since the DOI ratio of this array barely changes with depths[28], so unpolished crystal surface had to be used for ESR arrays to obtain a good DOI resolution. But for ESR array, the crystals in one direction cannot be resolved when the crystal size is down to $<$0.7 mm (array 2). For LSO array using Toray reflector and with small crystal size (~0.5 mm), polished crystal surface can be used to improve the light collection. The results show that for a LSO array using Toray reflector, polished crystal surface, 20 mm crystal length and 0.44 mm crystal size (array 3), all crystals can be clearly resolved and a DOI resolution of 2.1 mm was obtained. This was the smallest crystals that had been resolved for a dual-ended readout detector with 20 mm crystals length. The light collection can also be improved by reducing the crystal length. For a LSO array using Toray reflector, unpolished crystal surface, 10 crystal length and 0.5 mm crystal size, all crystals can be clearly resolved and the best DOI resolution of 1.4 mm was obtained. But the efficiency of this array is lower as compared to 20 mm array. Those detectors can be used to build small-animal PET scanners that simultaneously achieve high spatial resolution and high sensitivity.

References

[1] Bloomfield PM, Rajeswaran S, Spinks TJ, et al. The design and physical characteristics of a small animal positron emission tomograph [J]. Physics in Medicine and Biology, 1995, 40(6): 1105-1126.

[2] Vaquero JJ, Seidel J, Siegel S, et al. Performance characteristics of a compact position-sensitive LSO detector module [J]. IEEE Transactions on Medical

Imaging, 1998, 17(6): 967-978.

[3] Cherry SR, Shao Y, Silverman RW, et al. MicroPET: a high resolution PET scanner for imaging small animals [J]. IEEE Transactions on Nuclear Science, 1997, 44(3): 1161-1166.

[4] Lecomte R, Cadorette J, Rodrigue S, et al. Initial results from the Sherbrooke avalanche photodiode positron tomograph [J]. IEEE Transactions on Nuclear Science, 1996, 43(3): 1952-1957.

[5] Jeavons AP, Chandler RA, Dettmar CAR. A 3D HIDAC-PET camera with sub-millimetre resolution for imaging small animals [J]. IEEE Transactions on Nuclear Science, 1999, 46(3): 468-473.

[6] Tai YC, Ruangma A, Rowland D, et al. Performance evaluation of the microPET focus: a third-generation microPET scanner dedicated to animal imaging [J]. Journal of Nuclear Medicine, 2005, 46(3): 455-463.

[7] Yang Y, Tai YC, Siegel S, et al. Optimization and performance evaluation of the microPET II scanner for in vivo small-animal imaging [J]. Physics in Medicine and Biology, 2004, 49(12): 2527-2545.

[8] Seidel J, Vaquero JJ, Siegel S, et al. Depth identification accuracy of a three layer phoswich PET detector module [J]. IEEE Transactions on Nuclear Science, 1999, 46(3): 485-490.

[9] Wienhard K, Eriksson L, Eriksson M, et al. The ECAT HRRT: NEMA NEC evaluation of the HRRT system, the new high-resolution research tomograph [J]. IEEE Transactions on Nuclear Science, 2002, 49(5): 2085-2088.

[10] Inadama N, Murayama H, Hamamoto M, et al. 8-Layer DOI encoding of 3-dimensional crystal array [J]. IEEE Transactions on Nuclear Science, 2006, 53(5): 2523-2528.

[11] Wienhard K, Schmand M, Casey ME, et al. The ECAT HRRT: Performance and first clinical application of the new high resolution research tomograph [J]. IEEE Transactions on Nuclear Science, 2002, 49(1): 104-110.

[12] Tsuda T, Murayama H, Kitamura K, et al. A four-layer depth of interaction detector block for small animal PET [J]. IEEE Transactions on Nuclear Science, 2004, 51(5): 2537-2542.

[13] Orita N, Murayama H, Kawai H, et al. Three-dimensional array of scintillation crystals with proper reflector arrangement for a depth of interaction detector [J]. IEEE Transactions on Nuclear Science, 2005, 52(1): 8-14.

[14] Zhang N, Thompson CJ, Cayouette F, et al. A prototype modular detector design for high resolution positron emission mammography imaging [J]. IEEE Transactions on Nuclear Science, 2003, 50(5): 1624-1629.

[15] Dokhale PA, Silverman RW, Shah KS, et al. Performance measurements of a depth-encoding PET detector module based on position-sensitive avalanche photodiode read-out [J]. Physics in Medicine and Biology, 2004, 49(18): 4293-4304.

[16] Huber JS, Choong WS, Wang J, et al. Development of the LBNL positron emission mammography camera [J]. IEEE Transactions on Nuclear Science, 2003, 50(5): 1650-1653.

[17] Du H, Yang Y, Cherry SR. Measurements of wavelength shifting (WLS) fibre readout for a highly multiplexed, depth-encoding PET detector [J]. Physics in Medicine and Biology, 2007, 52(9): 2499-2514.

[18] Burr KC, Ivan A, Castleberry DE, et al. Evaluation of a prototype small animal PET detector with depth-of-interaction encoding [J]. IEEE Transactions on Nuclear Science, 2004, 51(4): 1791-1798.

[19] Vetter K, Burks M, Mihailescu L. γ-ray imaging with position-sensitive HPGe detectors [J]. Nuclear Instruments and Methods in Physics Research Section A: Accelerators, Spectrometers, Detectors and Associated Equipment, 2004, 525(1-2): 322-327.

[20] Wulf EA, Phlips BF, Johnson WN, et al. Germanium strip detector compton telescope using three-dimensional readout [J]. IEEE Transactions on Nuclear Science, 2003, 50(4): 1182-1189.

[21] Ling T, Lewellen TK, Miyaoka RS. Depth of interaction decoding of a continuous crystal detector

module [J]. Physics in Medicine and Biology, 2007, 52(8): 2213-2228.

[22] Lerche CW, Benlloch JM, Sanchez F, et al. Depth of γ-ray interaction within continuous crystals from the width of its scintillation light-distribution [J]. IEEE Transactions on Nuclear Science, 2005, 2(3): 560-572.

[23] Wang YC, Seidel J, Tsui BM, et al. Performance evaluation of the GE healthcare eXplore VISTA dual-ring small-animal PET scanner [J]. Journal of Nuclear Medicine, 2006, 47(11): 1891-1900.

[24] Levin CS, Hoffman EJ. Calculation of positron range and its effect on the fundamental limit of positron emission tomography system spatial resolution [J]. Physics in Medicine and Biology, 1999, 44(3): 781-799.

[25] Stickel JR, Cherry SR. High-resolution PET detector design: modelling compnents of intrinsic spatial resolution [J]. Physics in Medicine and Biology, 2005, 50(2): 179-195.

[26] España S, Marcinkowski R, Keereman V, et al. DigiPET: sub-millimeter spatial resolution small-animal PET imaging using thin monolithic scintillators [J]. Physics in Medicine and Biology, 2014, 59(13): 3405-3420.

[27] Yamamoto S, Watabe H, Kanai Y, et al. Development of an ultrahigh resolution Si-PM based PET system for small animals [J]. Physics in Medicine and Biology, 2013, 58(21): 7875-7888.

[28] Yang YF, Dokhale PA, Silverman RW, et al. Depth of interaction resolution measurements for a high resolution PET detector using position sensitive avalanche photodiodes [J]. Physics in Medicine and Biology, 2006, 51(9): 2131-2142.

[29] Janecek M, Moses WW. Optical reflectance measurements for commonly used reflectors [J]. IEEE Transactions on Nuclear Science, 2008, 55(4): 2432-2437.

[30] Shah KS, Grazioso R, Farrell R, et al. Position sensitive APDs for small animal PET imaging [J]. IEEE Transactions on Nuclear Science, 2004, 51(1): 91-95.

[31] McClish M, Dokhale P, Christian J, et al. Performance measurements of CMOS position sensitive solid-state photomultipliers [J]. IEEE Transactions on Nuclear Science, 2010, 57(4): 2280-2286.

[32] Yang YF, Wu YB, Farrell R, et al. Signal and noise properties of position-sensitive avalanche photodiodes [J]. Physics in Medicine and Biology, 2011, 56(19): 6327-6336.

[33] Judenhofer MS, Pichler BJ, Cherry SR. Evaluation of high performance data acquisition boards for simultaneous sampling of fast signals from PET detectors [J]. Physics in Medicine and Biology, 2005, 50(1): 29-44.

[34] James SS, Yang YF, Wu YB, et al. Experimental characterization and system simulations of depth of interaction PET detectors using 0.5 mm and 0.7 mm LSO arrays [J]. Physics in Medicine and Biology, 2009, 54(14): 4605-4619.